An Optimizing Diffusion Kernel-Based Binary Encoding Strategy With Genetic Algorithm for Fringe Projection Profilometry

Jiangping Zhu, Changhui Zhu, Pei Zhou, Zhoumiao He, and Di You

***Abstract*— The binary encoding fringe projection profilometry has the potential of achieving high-speed 3-D measurement. Error diffusion is one of the most widely investigated binary encoding techniques. However, the existing error diffusion usually utilizes the same diffusion kernel to encode sinusoidal (S) fringe patterns without considering the fringe pitch-widths, leading to inevitable measurement error due to the demodulated phase error. In this article, a fringe binary encoding strategy based on genetic algorithm is proposed to reduce the phase error recovered by the temporal phase unwrapping (TPU) method. We design an optimization equation that combines phase error and intensity error to calculate the encoding error, which ensures that the optimized diffusion kernel is robust to defocusing changes. Both simulation and experiments have proved the effectiveness and accurateness of the proposed method. Comparative experiments indicate that the extracted phase error is greatly reduced for two types of extensively adopted TPU methods at different defocusing levels. Especially for multi wavelength method, the phase error can be reduced by up to 68%.**

***Index Terms*— Absolute phase retrieval, binary encoding, error diffusion, fringe structured light, genetic algorithm (GA).**

I. Introduction

FRINGE projection profilometry (FPP) [1], [2] has broad application prospects in various fields, such as defect detection [3]–[5], reverse engineering [6], cultural heritage protection [7], and biomedicine, due to its versatilities of simple structure, non-contact, low cost, high accuracy, and high speed. The FPP analyzes the phase information of distorted fringe images captured and maps it to the 3-D information of objects. Phase shifting algorithm (PSA) is one of the important methods of demodulating phase. The wrapped phase is within the range of $(-\pi, \pi)$ with 2π phase discontinuities because of the arc tangent operation in PSA, so the phase unwrapping is necessary to obtain the continuous phase distribution. It can be divided into two categories: temporal phase unwrapping (TPU) [8]–[11] and spatial phase unwrapping (SPU) [12]. Compared with SPU, TPU method has been widely adopted in sinusoidal (S) structured light illumination 3-D measurement practices on account of its overwhelming advantages of high accuracy and the reliability of unwrapping the phase distorted by complex profiles like large spatial discontinuity and separation. SPU depends on the phase values of neighboring pixels, and the phase error will accumulate through the path, leading to its disability of effectively measuring objects with complex surface profiles. In contrast, TPU extracts the absolute phase of each pixel independently but requires projecting more fringe patterns of different frequencies to offer the fringe orders information. For the improvement of the measurement efficiency, projecting binary fringe patterns [11] via commercial digital projectors enables high-speed and flexible light field projection. Under the limitation of projector refresh rate (typically 120 Hz), defocusing the projection of binary fringe patterns instead of 8-bit S fringe patterns, which is able to greatly increase the measurement speed and avoid the influence of projector nonlinearity on the phase retrieval accuracy.

However, the binary encoding will inevitably introduce high-frequency components (encoding error) and will bring the phase error into the final 3-D measurement result. Various methods have been presented for patterns binary encoding: pulsewidth modulation (PWM), dithering, and optimization-based methods. The PWM, such as S PWM proposed by Ayubi *et al.* [13] and optimal PWM proposed by Wang and Zhang [14], is optimized only in 1-D, which fails to produce a high-performance 3-D measurement when fringe patterns have a wide pitch-width. The dithering methods mainly involve random dithering [15], ordered dithering [16], and error diffusion [17]. Compared with other methods, error diffusion method spreads the remaining errors multiplied by a weight to surrounding pixels of the currently processing pixel in implementing patterns encoding, and the accuracy can be significantly improved when the fringe period-width is large. Among them, the Floyd–Steinberg (F) method has been widely used due to its good performance in binary encoding. However, the F method was originally determined empirically for photograph processing, making it inevitable that careful optimization needs to be considered for S patterns encoding.

The optimization-based methods usually optimize the whole pattern [18] or the pattern block [19]–[22]. The former is

Manuscript received October 26, 2021; revised March 17, 2022; accepted March 31, 2022. Date of publication April 20, 2022; date of current version May 6, 2022. This work was supported in part by the National Natural Science Foundation of China under Grant 61901287 and Grant 62101364; in part by the Key Research and Development Program of Sichuan Province under Grant 2022YFG0053 and Grant 2021YFG0195; in part by the Major Science and Technology Projects of Sichuan Province under Grant 2019ZDZX0039 and Grant 2018GZDZX0029; in part by the China Postdoctoral Science Foundation under Grant 2021M692260; in part by the Key Laboratory of Fundamental Science for National Defense on Vision Synthetization and Graphic Image, Sichuan University, under Grant 2021SCUVS006; and in part by the Fundamental Research Funds for the Central Universities under Grant 2021SCU12049. The Associate Editor coordinating the review process was Md. Moinul Hossain. *(Corresponding author: Pei Zhou.)*

The authors are with the College of Computer Science and the National Key Laboratory of Fundamental Science on Synthetic Vision, Sichuan University, Chengdu 610065, China (e-mail: zjp16@scu.edu.cn; 2625693102@qq.com; michille78@163.com; scusws@163.com; youdi_scu@163.com).

Digital Object Identifier 10.1109/TIM.2022.3168900

inflexible to the change of the image resolution, while the latter requires the fringe pitch-width to be divisible by the number N of phase shifting. The objective function for optimization can be carried out in intensity domain [18], phase domain [20], frequency domain [19], or multiobjective strategy [21]. Recently, Zhou *et al.* [26] presented a kernel-optimized dithering technique on the basis of the F method. It has the ability of generating high-quality fringe patterns, but the weight coefficients still remain constant for different fringe pitch-widths. Characteristics of different fringe patterns (e.g., different fringe pitch-widths) can affect measurement accuracy [27], [28]. Encoding methods with shared diffusion kernel cannot always obtain the binary fringe pattern with the lowest encoding error, which affects the absolute phase retrieval accuracy synthesized by the TPU method [29].

In this study, we present a novel optimization strategy based on genetic algorithm (GA) to optimize error diffusion kernel coefficients for different fringe pattern pitch-widths. In addition, indirect optimization of binary patterns through error diffusion kernel can flexibly cope with the patterns resolution changes under encoding. We optimize the diffusion kernels for the fringe pattern of each pitch-width separately, instead of sharing a diffusion kernel for all the fringe patterns of different pitch-widths adopted in TPU method. A new optimization function is designed to help solve the diffusion kernels. Both phase error and intensity error are included in the optimization function, which greatly enhances the robustness of the optimization result. Simulated and experimental results confirm that the proposed method has the ability of significantly improving the accuracy of absolute phase recovered by two typical TPU methods.

The remainder of this article is organized as follows. Section II briefly introduces the relevant principles and presents optimization strategy in detail. Sections III and IV describe the simulation and experimental results, respectively. Finally, some conclusions are drawn in Section V.

II. Principle

A. Error Diffusion

Error diffusion has been widely used in image binary encoding, which encodes continuous S pattern (typically 8-bit) into binary ones with gray intensity of only 0 and 1 (or 255). With a defocusing of proper extent, the encoded pattern can demonstrate the original pattern information as much as possible, and greatly reduce the number of bits. Fig. 1 shows the general principle of the binary encoded S pattern with pitch-width $T = 36$ pixels encoded by F method. There is a slight difference in the intensity profile between the encoded pattern and the origin S pattern.

The error diffusion process can be expressed as

$$\mathbf{I}_{\mathrm{b}}(i,j) = \mathrm{binary}\left(\mathbf{I}_s(i,j) + \sum_{i}^{2}\sum_{j}^{3}\mathbf{W}(x,y)\mathbf{e}(i-x,j-y)\right) \tag{1}$$

and the classical F diffusion kernel is

$$\mathbf{W}_{\mathrm{F}}(x,y) = \frac{1}{16}\begin{bmatrix} \sim & * & 7 \\ 3 & 5 & 1 \end{bmatrix} \tag{2}$$

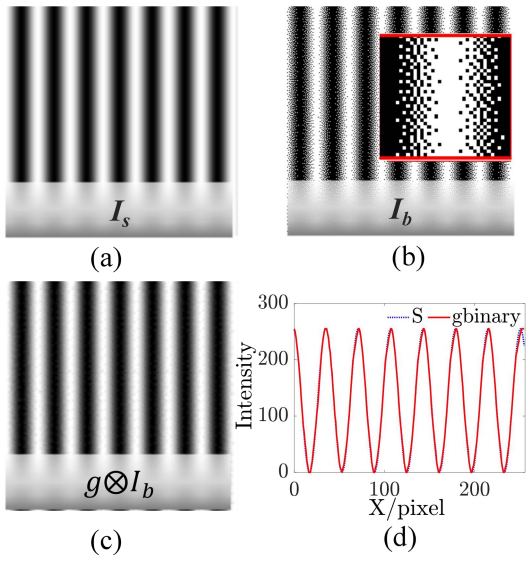

Fig. 1. Error diffusion mechanism. (a) Original S pattern. (b) Pattern encoded by F method. (c) I_b after Gaussian filtering, g is a Gaussian function, and $\otimes$ is a convolution operation. (d) 128th gray profile of (a) and (c), named "S" and "gbinary," respectively.

where $\boldsymbol{I}_b$ represents the binary pattern; binary ( ) as a threshold function that sets the pixel value to 255 or 0 according to the threshold (127); $\boldsymbol{I}_{\mathbf{s}}$ is the S pattern to be encoded, e represents the residual error between $\boldsymbol{I}_b$ and $\boldsymbol{I}_{\mathbf{s}}$, W is the diffusion kernel, and (i, j) (x, y) are the pixel coordinate, $*$ represents the pixel under processing, and $\sim$ is the processed pixel.

The coefficients included in the error diffusion kernel will have a direct influence on the final binary performance. A novel binary encoding method is therefore desired to generate diffusion kernels that enable us to obtain accurate absolute phase with less phase error recovered through TPU method.

B. Temporal Phase Unwrapping

The TPU method needs to project multiple frequencies (typically three) of temporally related fringe patterns, and the absolute phase can be unwrapped according to the phase relationship between them. This category of TPU method can be divided into three subgroups: multifrequency (MF) (hierarchical) methods [23], multiwavelength (MW) (heterodyne) methods [24], and number theoretical approaches [25]. The first two methods with three different fringe frequencies are usually more widely utilized in 3-D measurement activities for the balance between measurement accuracy and efficiency; thus, we take them into consideration to optimize the error diffusion kernel.

The MF method projects three groups of patterns with fringe frequencies of 1, f, and f^2. The continuous phase of fringe pattern with frequency of 1 is equal to its wrapped phase. The fringe order of higher-frequency fringe patterns can be determined with the aid of the lower-frequency unwrapped phase. The phase unwrapping process can be expressed as

$$\begin{cases} \phi_1 = \varphi_1 \\ \phi_i = 2\pi\,\mathrm{Round}\left(\dfrac{f\phi_{i-1} - \varphi_i}{2\pi}\right) + \varphi_i, \quad i = 2, 3 \end{cases} \tag{3}$$

where Round ( ) takes the closest integer, ϕ represents the unwrapped phase, φ is the wrapped phase, $i = 0$ is the lowest frequency, and $i = 2$ indicates the highest frequency.

Differing from MF method, the MW method requires projecting three groups of fringe patterns with a close pitch-width. By heterodyning the three fringe patterns with pitch-widths T_1, T_2, and T_3, the fringe pattern with wider pitch-width T_{123} can be obtained. Therefore, the pitch-widths (T_1, T_2, and T_3) of the fringes should be selected appropriately to yield a fringe wider than the original ones and obtain the unwrapped phase. Taking three frequencies as an example, the heterodyning process can be expressed as (5). Let the wrapped phases corresponding to the fringe patterns of pitch-widths T_1, T_2, and T_3 be φ_1, φ_2, and φ_3, respectively. φ_{12} can be obtained by heterodyning φ_1 and φ_2, and φ_{23} can be obtained by heterodyning φ_2 and φ_3. Finally, φ_{12} and φ_{23} can be used to obtain the unwrapped phase φ_{123} that contains 2π corresponding to only a single pitch-width by the heterodyning method. The unwrapped absolute phase φ_{123} corresponding to T_{123} is viewed as the lowest-frequency phase to assist the higher-frequency phase unwrapping

$$T_{123} = \frac{T_1 T_2^2 T_3}{T_2^2(T_1 + T_3) - 2T_1 T_2 T_3}, \quad T_1 > T_2 > T_3. \tag{4}$$

$$\varphi_{ij} = \begin{cases} \varphi_j - \varphi_i, & \text{if } \varphi_j \geq \varphi_i \\ \varphi_j - \varphi_i + 2\pi, & \text{else.} \end{cases} \tag{5}$$

In this article, three-step PSA is adopted to demodulate the wrapped phase considering the measurement efficiency. The final absolute phase Φ synthesized by the unwrapped phases of three frequency fringe patterns with least squared weight [21]

$$\Phi = \frac{\sum_{i=1}^{3} f_i \phi_i}{\sum_{i=1}^{3} f_i^2}. \tag{6}$$

C. Optimization Strategy of Binary Encoding

Because the optimization process of fringe binary encoding can be classified as the non-deterministic polynomial problem, most studies have resolved it by employing global search (GS) algorithm, particle swarm optimization (PSO) algorithm, and GA. GS has stable optimization results, but is extremely time-consuming. PSO comprehensively considers the individual optimal value and the global optimal value. PSO is mainly applied to solve continuous problems, and the research maturity of algorithm convergence is weaker than that of GA. GA obtains an optimal solution to a given computational problem through selection, crossover, and mutation of chromosomal genes in biological evolution, which is far more powerful and efficient than GS and PSO algorithms. Meanwhile, GA has the advantages of simple structure, easy implementation, good fault tolerance, and fewer optimization parameters [30]. Therefore, this article utilizes GA to optimize the error diffusion kernel coefficients $(\omega_1, \omega_2, \omega_3, \omega_4)$ in the following equation:

$$\mathbf{W}_{\text{opt}} = \frac{1}{\sum_{i=1}^{4} \omega_i} \begin{bmatrix} - & * & \omega_1 \\ \omega_2 & \omega_3 & \omega_4 \end{bmatrix}. \tag{7}$$

The optimized kernel is suitable for the specific fringe patterns applied in TPU method, so that the final absolute phase error of the encoded fringe patterns is lower than that of the traditional error diffusion strategy.

The phase-based optimization method is capable of yielding high-quality phase but it is sensitive to the extent of defocusing [18]. This problem can be solved if both phase error and intensity error are considered simultaneously. The root mean square error (RMSE) is employed to evaluate the error level, I_1 is the reference image and I_2 is the image to be evaluated, and $c \times r$ is the size of image

$$\text{RMSE}(I_1,\ I_2) = \sqrt{\frac{\sum (I_1 - I_2)^2}{c \times r}}. \tag{8}$$

We introduce linear fitting to obtain the weight ratio of intensity error and phase error, which aims to synthesize the comprehensive encoding error of the given pitch-width fringe patterns involved in TPU method.

First, the S patterns are binary-encoded via F method and are blurred by a Gaussian filter (with size k) for each fringe pitch-width T. The phase error E_p and intensity error E_i of the binary pattern are calculated according to the following equations:

$$E_{\text{p}} = \text{RMSE}(\Phi_s,\ \Phi_b). \tag{9}$$

$$E_i = \text{RMSE}(I_s,\ g \otimes I_b). \tag{10}$$

Second, the weight function $\beta(T, k)$ can be obtained when the normalized E_p is equal to the normalized E_i, namely, $\beta \cdot E_p/2\pi = (1 - \beta) \cdot E_i/2I_m$, where I_m represents the maximum gray value of image and $\beta(T, k) \in (0,\ 1)$. We used six pitch-widths of $T = 20, 40, \ldots, 120$ pixels, and five Gaussian window sizes of $k = 5, 7, \ldots, 13$. Linear fitting is performed on the obtained 30 triples, and the weight function $\beta(T, k)$ related to fringe pitch-width T and the size of Gaussian window k is established. Subsequently, the composite error E_T of the encoding pattern is expressed by the following equation:

$$E_T = \beta(T, k)\frac{E_{\text{p}}}{2\pi} + (1 - \beta(T, k))\frac{E_{\text{i}}}{2I_{\text{m}}}. \tag{11}$$

Finally, for the fringe patterns of different frequencies involved in TPU method, a diffusion kernel with the smallest encoding error is optimized to make the final encoding error E_{all} [see (12)] as small as possible. The main process of the proposed pattern binary encoding optimization strategy is shown in Fig. 2

$$E_{\text{all}} = \sum_{i=1}^{3} E_{T_i}. \tag{12}$$

The optimization strategy can be elaborated as follows.

Step 1 (Initialization): Randomly generate initial individuals, each of which is composed of four genes, corresponding to the coefficients $(\omega_1, \omega_2, \omega_3, \omega_4)$ to be optimized in the error diffusion kernel, and the code length of each gene is 6 bits. We simply set the number of individuals to $2^{\text{length ofeachgene}}$ and always keep the F method diffusion kernel in the initial population.

Step 2 (Error Calculation): Each individual is converted into a diffusion kernel, and the bidirectional diffusion path [22] is used to encode the S pattern groups to eliminate the

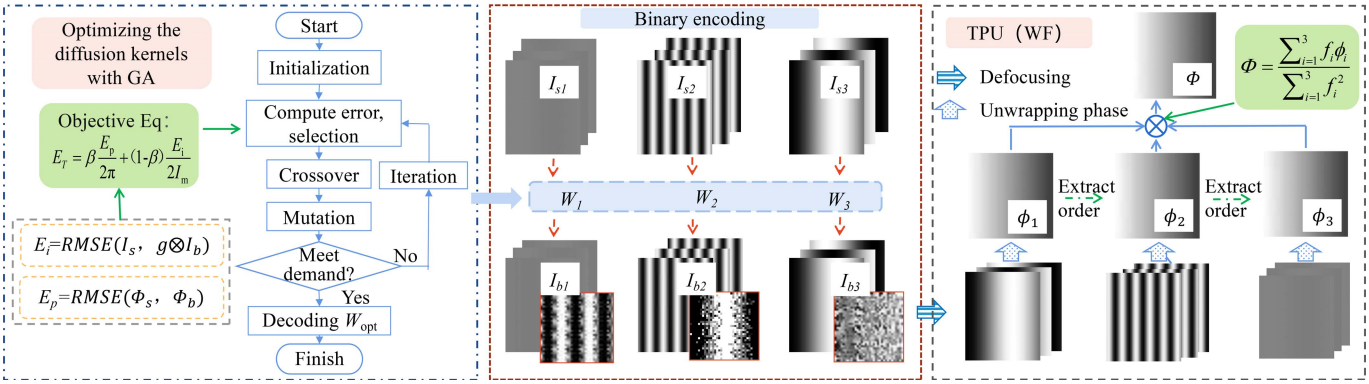

Fig. 2. Flowchart of the proposed method.

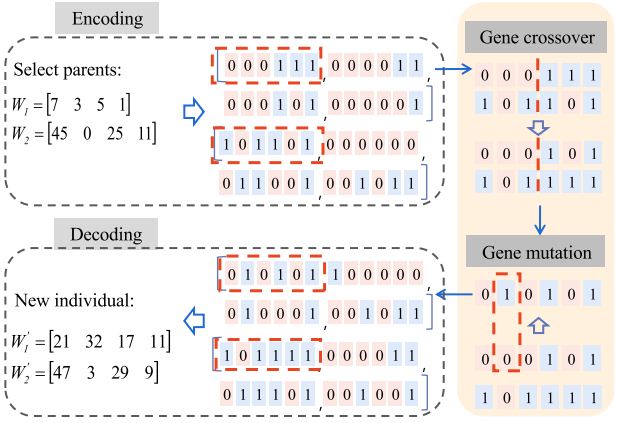

Fig. 3. Schematic of individual crossover and mutation.

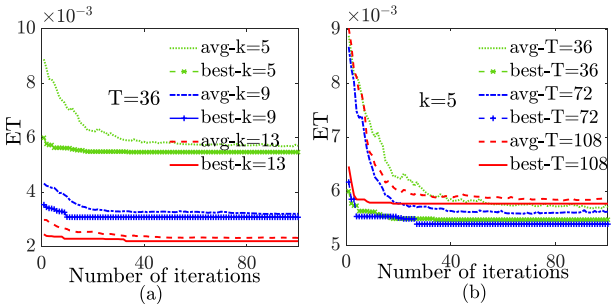

Fig. 4. Convergence process of error diffusion kernel optimization. (a) $T = 36$ pixel and $k = 5$, 9, and 13 pixels. (b) $k = 5$ pixel and $T = 36$, 72, and 108 pixel.

accumulation of errors in a certain direction. According to Section II-C, the individuals' error is computed.

Step 3 (Selection): Different weights are assigned to individuals in a reverse order of E_T error, and crossover targets are selected according to proportion selection method.

Step 4 (Crossover): Randomly select a position and crossover each gene of two individuals according to crossover probability. For each iteration, the optimal individual is retained. In order to produce a more abundant population, the probability of crossover is set as 100%. Before crossover, the individual will be encoded into a binary mode, as shown in Fig. 3.

Step 5 (Mutation): Setting the mutation probability as 0.3%, the mutation point is randomly selected for gene mutation, and generates the next generation of individuals.

Step 6 (Iteration): Update the current minimum E_T and the corresponding individual. If the iteration converges, skip to step 7, otherwise return to step 2. Since the iteration always converges before 40 times, shown in Fig. 4, we directly set the maximum number of iterations to 40.

Step 7 (Patterns Generation): The individual corresponding to the recorded minimum E_T is decoded to an error diffusion kernel, which is used for the binary encoding of a given frequency S pattern of arbitrary image resolution.

Step 8 (Repeat): Repeat the above process for three frequency fringe patterns to yield their corresponding diffusion kernels W_1, W_2, and W_3 in Fig. 2.

III. Simulations

Simulations are carried out to evaluate the performance of the proposed optimization strategy. For comparison, the phase errors achieved with the fringe patterns encoded by F method and the method proposed in [26] (abbreviated to H hereafter) are also comparatively evaluated. Various defocusing levels are simulated by filtering the binary encoding patterns with a size of $k \times k$ Gaussian filter and standard derivation σ equal to $k/3$, where $k \in \{5, 9, 13\}$.

Utilizing the kernel obtained by the optimization strategy described in Section II-C when $T = 36$ pixels, S patterns of other pitch-widths are encoded, and the results are shown in Fig. 5. It can be concluded that the phase RMSE of $T = 36$ pixels is always lower than that of other pitch-widths as the defocusing level increases. Coincidentally, similar results can be obtained when the pitch-width is changed, indicating that an optimum kernel is definitely existed in a given pitch-width via our proposed encoding strategy.

When MF is adopted to unwrap the absolute phase, the fringe pitch-widths are 1176, 168, and 24 pixels, while 24, 27, and 30 pixels when using MW method. The phase RMSE is summarized in Table I. Fig. 6 shows the 530th row cross section of absolute phase error between the computed results by each method and the ground truth. It can be clearly identified that the phase error of the proposed method (Ours) is invariably the smallest under different sizes of Gaussian filtering, whatever it is unwrapped by MF or MW.

As the Gaussian filter size gradually increases, the phase RMSE via the proposed method is reduced by 72.15%,

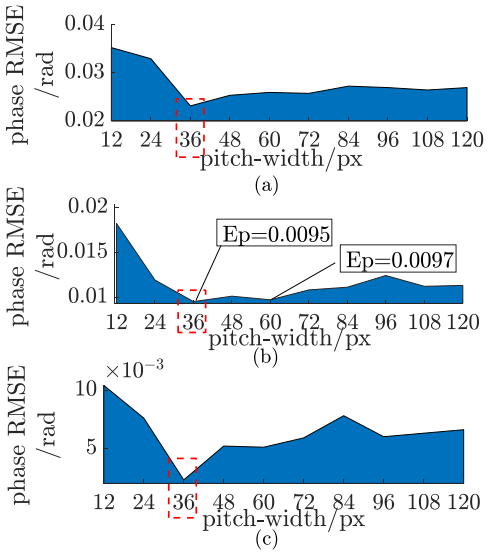

Fig. 5. Phase RMSE of encoding S patterns of different pitch-widths under Gaussian filters (pixels). (a) $k = 5 \times 5$. (b) $k = 9 \times 9$. (c) $k = 13 \times 13$.

TABLE I
ABSOLUTE PHASE RMSE OF PLANE IN SIMULATION(RAD)

Method	MF			MW		
	σ=5/3	σ=9/3	σ=13/3	σ=5/3	σ=9/3	σ=13/3
F [17]	0.0554	0.0507	0.0500	0.0420	0.0402	0.0400
H [26]	0.0293	0.0119	0.0077	0.0151	0.0061	0.0035
Ours	0.0154	0.0070	0.0036	0.0096	0.0034	0.0024

84.89%, and 92.86% compared with that of F method, and the phase RMSE is reduced by 47.36%, 35.43%, and 48.81% relative with the H method when MF is adopted.

For MW, the phase RMSE derived from the proposed method is reduced by 77.06%, 91.44%, and 94.10% in comparison with that of F method, while the phase RMSE is decreased by 36.22%, 43.42%, and 33.18% with H method. In general, it can be distinguished from Fig. 6, and the phase error of the proposed method is closer to zero, especially when the projector is nearly focused ($\sigma = 5/3$), indicating that ours method could have certain advantages like larger filed of depth in practical 3-D measurement activities without the projector' large defocusing.

IV. EXPERIMENTS

Experiments are conducted to evaluate the presented method by the establishment of a 3-D measurement system equipped with a Daheng mercury camera (model: MER-131-210U3M, resolution: 1024 × 1280 pixels) of a 16-mm focal length, a projector (DLP4500, resolution: 1140 × 912 pixels), and a computer for image capture and processing. The distance between the target plane and the projector is about 50 cm, and the optical axis of the projector used is approximately perpendicular to the target plane, and the angle between the camera's and the projector's optical axis is about 30°.

We refer to the method proposed in [32] to evaluate the defocusing level of the experimental system. For simplicity, we implement a perspective transformation on the captured images. Here, the 1-D Gaussian function is taken as the

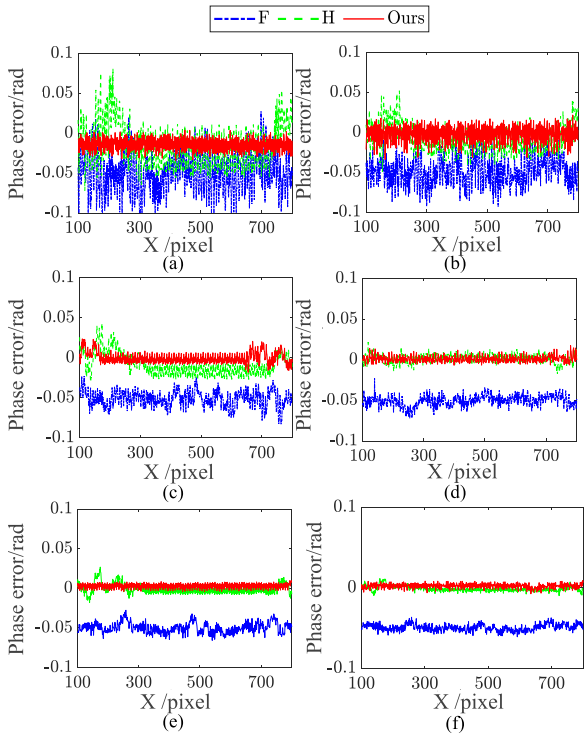

Fig. 6. Comparison of the absolute phase errors achieved by F method, H method, and the proposed method (Ours), with Gaussian filters (pixels) (a) and (b) $k = 5 \times 5$. (c) and (d) $k = 9 \times 9$. (e) and (f) 13 × 13. (a), (c), and (e) MF method. (b), (d), and (f) MW method.

defocus function model. By analyzing the change of boundary gray value of square wave fringe before and after projecting, the defocusing level of the current system can be roughly estimated. Fig. 7(a) demonstrates a square wave fringe pattern of $T = 72$ pixels to be projected. The changes of gray value are shown in Fig. 7(d). Different defocusing levels result in different reductions in the contrast of the square wave fringe borders. Fig. 7(b) shows the captured square wave fringe image after defocusing at $\sigma \approx 2.25$. In order to reduce the estimated error, the current defocusing level of the projector is computed with the fringe border of 100 pixels located within the center area of the image, as shown by the red line segment in Fig. 7(a)–(c).

To quantitatively evaluate the performance of F method, H method, and the proposed method, a ceramic plane by adjusting different defocusing levels is tested. We compare the phase RMSE between the absolute phase recovered from the binary images via different encoded methods and the ideal phase. The ideal phase is obtained via a 12-step PSA with S patterns of the same frequencies, while three-step PSA is adopted for the remaining methods. An area of 300 × 300 pixels with no fringe order errors in the center of the fringe patterns projected, captured images, wrapped phase, absolute phase unwrapped by MF method, and the absolute error map for each method when $T = 24$ pixels, are shown in Fig. 8(a)–(e), respectively. It can be concluded that the phase RMSE ($E_p = 0.0260$ rd) of the proposed method is the lowest compared with 0.0514 rd of F method and 0.0307 rd of H method.

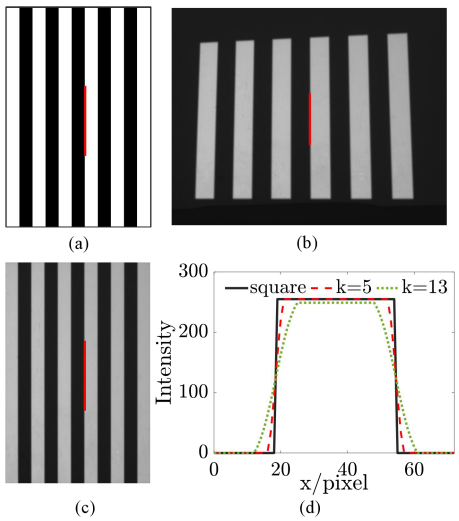

Fig. 7. (a) Square binary fringe pattern with $T = 72$ pixels to be projected. (b) Captured defocusing square binary fringe image at $\sigma \approx 2.25$. (c) Perspective transformation of the image in (b). The area of red line is used to estimate the defocusing level. (d) Effect of different defocusing levels on the gray values at the boundary of the square binary fringes.

TABLE II
ABSOLUTE PHASE RMSE BY MF (RAD)

σ	F [17]	H [26]	Ours
1.58	0.0563	0.0318	0.0289
2.25	0.0514	0.0307	0.0260
2.64	0.0536	0.0273	0.0247
3.50	0.0534	0.0262	0.0247
4.03	0.0545	0.0260	0.0251

TABLE III
ABSOLUTE PHASE RMSE BY MW (RAD)

σ	F [17]	H [26]	Ours
1.58	0.0525	0.0201	0.0171
2.25	0.0468	0.0205	0.0170
2.64	0.0505	0.0172	0.0163
3.50	0.0495	0.0169	0.0160
4.03	0.0504	0.0165	0.0161

Tables II and III, respectively, summarize the absolute phase RMSE by MF method and MW method as the defocusing level σ gradually increases (along the column direction) when the ceramic plane is tested. When $\sigma \approx 1.58$, projected patterns are generated by the kernel optimized under $k = 5$, $\sigma \approx 2.25$, and $\sigma \approx 2.64$ corresponding to $k = 9$, $\sigma \approx 3.04$, and $\sigma \approx 4.03$ corresponding to $k = 13$.

Obviously, the proposed method allows us to obtain more accurate absolute phase than the F method and the H method. For MW method, the percentage of error reduction is large than 60% compared with the F method, and the maximum can reach to 68.06%. Compared with the H method, the percentage can be reduced by up to 17.07%. Regardless of defocusing level, totally the calculated phase RMSE of the patterns encoded by ours method is the lowest.

In order to further evaluate the proposed method, a complex object is employed to reconstruct the 3-D phase maps. The ground truth is obtained by subtracting the absolute phase

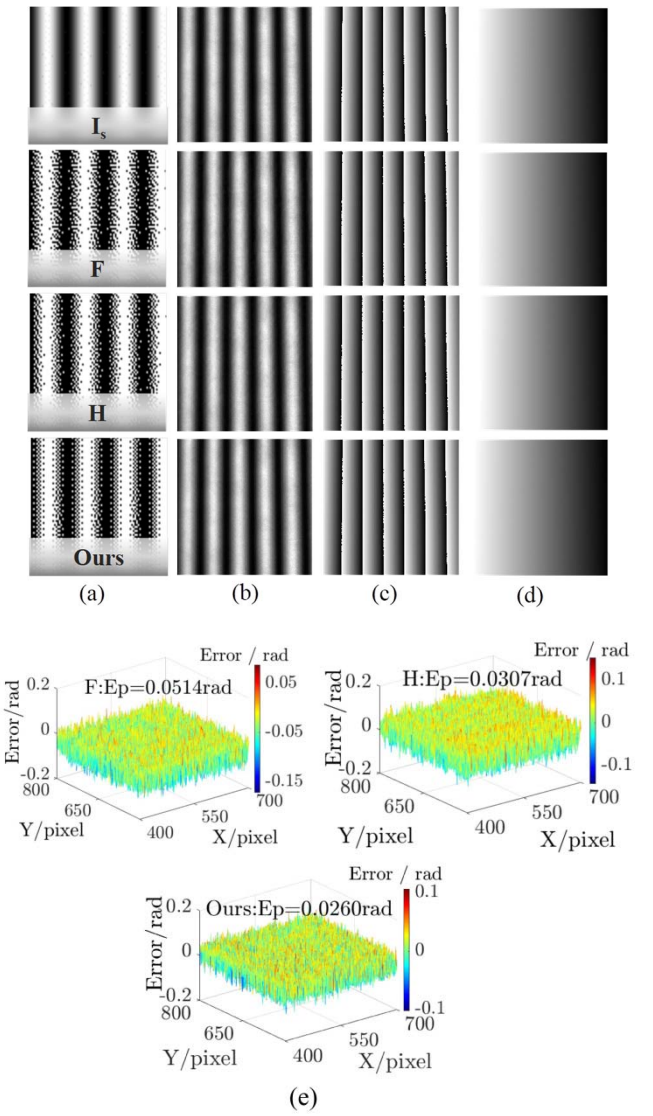

Fig. 8. Comparison of F method, H method, and the proposed method when the ceramic plane is tested. (a) Binary fringe patterns encoded by different methods with $T = 24$ pixels. (b) Captured images after defocusing at $\sigma \approx 2.25$. (c) Wrapped phase. (d) Absolute phase unwrapped by MF. (e) Absolute error relative to the ideal phase.

distorted by the reference plane from that of the deformed fringes image distorted by the tested mask via the projection of S patterns of the same frequencies. The ground truth is computed by 12-step PSA in comparison with three-step PSA for F, H, as well as our method. The defocusing level on the object differs in different depths; however, the optimized kernels can still adapt a certain range of defocusing changes due to the intensity error added in our optimization. We display parts of 3-D phase maps reconstructed by each method in Fig. 9. The 530th column crossed sections and partially enlarged plots from four methods are illustrated in Fig. 9(b) and (c), indicating that the retrieval phase via our method is closest to the ideal 3-D phase, with the smallest phase error, as shown in Fig. 9(d).

Furthermore, we select an area of 250 × 300 pixels with no fringe order errors in the center of the images to calculate the

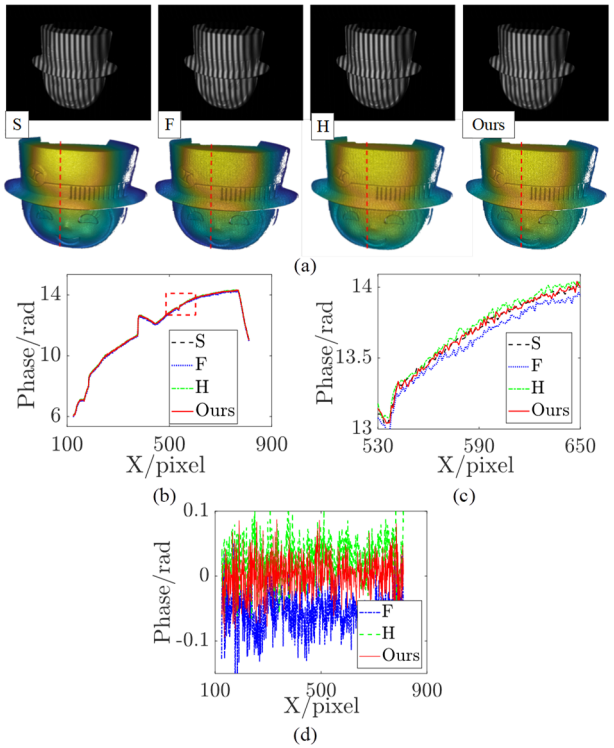

Fig. 9. (a) Distorted fringe images (the first row) and the corresponding 3-D phase maps (the second row) reconstructed, respectively, by S method, F method, H method, and the proposed method at $\sigma \approx 2.64$ ith WF method. (b) 530th column [red line in (a)] on the reconstructed 3-D phase maps. (c) Partially enlarged view of (b). (d) Error comparison between those encoding methods (F, H, and ours) relative to S method.

TABLE IV
ABSOLUTE PHASE RMSE OF A COMPLEX MASK RECONSTRUCTED BY MF (RAD)

σ	F [17]	H [26]	Ours
1.58	0.0537	0.0216	0.0193
2.25	0.0562	0.0313	0.0279
2.64	0.0561	0.0285	0.0258
3.50	0.0548	0.0284	0.0271
4.03	0.0520	0.0294	0.0273

TABLE V
ABSOLUTE PHASE RMSE OF A COMPLEX MASK RECONSTRUCTED BY MW (RAD)

σ	F [17]	H [26]	Ours
1.58	0.0585	0.0342	0.0313
2.25	0.0515	0.0199	0.0181
2.64	0.0523	0.0181	0.0170
3.50	0.0502	0.0183	0.0176
4.03	0.0476	0.0199	0.0175

phase RMSE, and the results are listed in Tables IV and V. For MW method, the phase RMSE of the proposed method is reduced by larger than 60% compared with the F method, except 46.5% when $\sigma \approx 1.58$, while it is approximately 4%–12% lower than that of the H method. Similar to the experimental results of the tested ceramic plane, the proposed method can achieve more accurate results in the absolute phase calculation of a complex object. The comparative experiments demonstrate that the proposed method enjoys the ability of always generating high-quality absolute phase even if the defocusing level changes with the depth of the tested object.

We encoded in MATLAB to optimize the diffusion kernel of the same resolution fringe pattern with a given fringe pitch-width $T = 24$ pixels. The H method took 3.81 h, while the algorithm proposed in this article takes 26.47, 27.07, and 372.04 s to optimize the fringe patterns of $T = 24$, 168, and 1176 pixels, respectively. The proposed method requires much less time while obtaining higher accuracy. But in order to achieve the purpose of high-speed measurement, we recommend offline optimization of the diffusion kernels and only need to call the existing results during measurement.

V. CONCLUSION

In this article, we present an error diffusion kernel optimization strategy for binary fringe pattern projection profilometry. The GA is utilized to optimize the error diffusion kernel coefficients, and the diffusion kernel with lower encoding error in a certain pitch-width is found for binary fringe pattern encoding. Distinguished from F methods and H method, the proposed method fully considers the pitch-widths of fringe patterns involved in the TPU method concretely adopted. Therefore, the absolute phase synthesized by the proposed method enjoys the highest accuracy. Both simulation and experimental results have proved that the proposed method is capable of effectively reducing the absolute phase error of two typical TPU methods under different defocusing levels, especially with the MW method.

The major drawback of the proposed method is that it costs a certain amount of time to optimize the diffusion kernel, but once the optimization is finished, the binary encoding can be implemented conveniently and for the given S pattern regardless of its image resolution. In future work, we will further study the impact of choosing different algorithms on binary graph optimization, and try to shorten the optimization time to achieve online optimization.

REFERENCES

[1] C. Zuo, S. Feng, L. Huang, T. Tao, W. Yin, and Q. Chen, "Phase shifting algorithms for fringe projection profilometry: A review," *Opt. Lasers Eng.*, vol. 109, pp. 23–59, Oct. 2018, doi: 10.1016/j.optlaseng.2018.04.019.

[2] S. Feng, L. Zhang, C. Zuo, T. Tao, Q. Chen, and G. Gu, "High dynamic range 3D measurements with fringe projection profilometry: A review," *Meas. Sci. Technol.*, vol. 29, no. 12, Dec. 2018, Art. no. 122001.

[3] H. Wang, J. Ma, H. Yang, F. Sun, Y. Wei, and L. Wang, "Development of three-dimensional pavement texture measurement technique using surface structured light projection," *Measurement*, vol. 185, Nov. 2021, Art. no. 110003.

[4] S. Kang and I. C. Ume, "Dynamic digital fringe projection technique for measuring the warpage of unpainted PBGA packages and boards," *Int. J. Adv. Manuf. Technol.*, vol. 96, nos. 9–12, pp. 3235–3249, Jun. 2018.

[5] Y. Wang, H. Zhao, X. Li, and H. Jiang, "High-accuracy 3-D sensor for rivet inspection using fringe projection profilometry with texture constraint," *Sensors*, vol. 20, no. 24, p. 7270, Dec. 2020.

[6] N. Farahi, M. Abolbashari, J. Babaie, J. Ziegert, R. Porras-Aguilar, A. Davies, and F. Farahi, "Inverse projected-fringe technique for measurement of dimensions and surface profile of axisymmetric objects," *Meas. Sci. Technol.*, vol. 30, Nov. 2018, Art. no. 015009.

[7] L. Gomes, O. Regina Pereira Bellon, and L. Silva, "3D reconstruction methods for digital preservation of cultural heritage: A survey," *Pattern Recognit. Lett.*, vol. 50, pp. 3–14, Dec. 2014.

[8] C. Zuo, L. Huang, M. Zhang, Q. Chen, and A. Asundi, "Temporal phase unwrapping algorithms for fringe projection profilometry: A comparative review," *Opt. Lasers Eng.*, vol. 85, pp. 84–103, Oct. 2016, doi: 10.1016/j.optlaseng.2016.04.022.

[9] X. Chen *et al.*, "Two-digit phase-coding strategy for fringe projection profilometry," *IEEE Trans. Instrum. Meas.*, vol. 70, pp. 1–9, 2021.

[10] Y. Zheng, Y. Jin, M. Duan, C. Zhu, and E. Chen, "Joint coding strategy of the phase domain and intensity domain for absolute phase retrieval," *IEEE Trans. Instrum. Meas.*, vol. 70, 2021, Art. no. 7004908, doi: 10.1109/TIM.2021.3088471.

[11] J. Zhu, P. Zhou, X. Su, and Z. You, "Accurate and fast 3D surface measurement with temporal-spatial binary encoding structured illumination," *Opt. Exp.*, vol. 24, no. 25, p. 28549, Dec. 2016, doi: 10.1364/oe.24.028549.

[12] S. Lv, Q. Sun, J. Yang, Y. Jiang, F. Qu, and J. Wang, "An improved phase-coding method for absolute phase retrieval based on the path-following algorithm," *Opt. Lasers Eng.*, vol. 122, pp. 65–73, Nov. 2019, doi: 10.1016/j.optlaseng.2019.05.024.

[13] G. A. Ayubi, J. A. Ayubi, J. M. Di Martino, and J. A. Ferrari, "Pulse-width modulation in defocused three-dimensional fringe projection," *Opt. Lett.*, vol. 35, no. 21, pp. 3682–3684, 2010, doi: 10.1364/ol.35.003682.

[14] Y. Wang and S. Zhang, "Optimal pulse width modulation for sinusoidal fringe generation with projector defocusing," *Opt. Lett.*, vol. 35, no. 24, pp. 4121–4123, 2010, doi: 10.1364/ol.35.004121.

[15] W. Purgathofer, R. F. Tobler, and M. Geiler, "Forced random dithering: Improved threshold matrices for ordered dithering," in *Proc. 1st Int. Conf. Image Process.*, Nov. 1994, pp. 1032–1035, doi: 10.1109/ICIP.1994.413512.

[16] B. E. Bayer, *An Optimum Method for Two-Level Rendition of Continuous-Tone Pictures*. New York, NY, USA: IEEE Press, 1973, pp. 2611–2615.

[17] R. Floyd and L. Steinberg, "An adaptive algorithm for spatial gray scale," *Proc. Soc. Inf. Display*, vol. 17, pp. 75–77, Jan. 1975.

[18] J. Dai, B. Li, and S. Zhang, "Intensity-optimized dithering technique for three-dimensional shape measurement with projector defocusing," *Opt. Lasers Eng.*, vol. 53, pp. 79–85, Feb. 2014, doi: 10.1016/j.optlaseng.2013.08.015.

[19] N. Cai, Z. Chen, X. Cao, and B. Lin, "Optimized dithering technique in frequency domain for high-quality three-dimensional depth data acquisition," *Chin. Phys. B*, vol. 28, no. 8, Aug. 2019, Art. no. 084202, doi: 10.1088/1674-1056/28/8/084202.

[20] N. Cai, Z. Chen, B. Lin, and X. Cao, "Genetic method to optimize dithering technique in phase domain for high-quality binary fringe generation," *Acta Photonica Sinica*, vol. 48, no. 8, 2019, Art. no. 811002, doi: 10.3788/gzxb20194808.0811002.

[21] N. Cai, Z. Chen, X. Cao, and B. Lin, "Multi-objective strategy to optimize dithering technique for high-quality three-dimensional shape measurement," *Chin. Phys. B*, vol. 28, no. 10, 2019, Art. no. 104210, doi: 10.1088/1674-1056/ab427b.

[22] A. Silva, A. Muñoz, J. L. Flores, and J. Villa, "Exhaustive dithering algorithm for 3D shape reconstruction by fringe projection profilometry," *Appl. Opt.*, vol. 59, no. 13, p. D31, May 2020, doi: 10.1364/ao.381924.

[23] H. Hu *et al.*, "A combined binary defocusing technique with multi-frequency phase error compensation in 3D shape measurement," *Opt. Lasers Eng.*, vol. 124, Jan. 2020, Art. no. 105806, doi: 10.1016/j.optlaseng.2019.105806.

[24] Z. Yu, J. Liu, H. Yang, B. Huang, and Y. Jian, "A multifrequency heterodyne phase error compensation method for 3D reconstruction," *J. Sensors*, vol. 2020, pp. 1–10, Aug. 2020, doi: 10.1155/2020/8833305.

[25] W. Yin *et al.*, "High-speed three-dimensional shape measurement using geometry-constraint-based number-theoretical phase unwrapping," *Opt. Lasers Eng.*, vol. 115, pp. 21–31, Apr. 2019, doi: 10.1016/j.optlaseng.2018.11.006.

[26] P. Zhou, N. Cai, T. Wang, X. Cao, and B. Lin, "High-quality 3D shape measurement by kernel-optimized high sinusoidal similarity dither patterns," *Appl. Opt.*, vol. 59, no. 34, pp. 10645–10650, Dec. 2020, doi: 10.1364/ao.403832.

[27] Z. Zheng, J. Gao, Y. Zhuang, L. Zhang, and X. Chen, "High dynamic defocus response method for binary defocusing fringe projection profilometry," *Opt. Lett.*, vol. 46, pp. 3749–3752, Nov. 2021.

[28] J. Yu, N. Gao, Z. Zhang, and Z. Meng, "High sensitivity fringe projection profilometry combining optimal fringe frequency and optimal fringe direction," *Opt. Lasers Eng.*, vol. 129, Jun. 2020, Art. no. 106068.

[29] W. Zhao, W. Chen, and X. Su, "The comparison of several time phase unwrapping methods," *J. Sichuan Univ. (Natural Sci. Ed.)*, vol. 53, no. 1, pp. 110–117, 2016.

[30] D. Lichti, "A comparison of simulated annealing, genetic algorithm and particle swarm optimization in optimal first-order design of indoor TLS networks," *ISPRS Ann. Photogramm., Remote Sens. Spatial Inf. Sci.*, vol. 4, pp. 75–82, Sep. 2017.

[31] P. Zhou, J. Zhu, H. Jing, Z. Duan, S. An, and Y. Guo, "Design and experimental study of sinusoidal structured light mask with 'S' shaped binary coding," *Laser Optoelectron. Prog.*, vol. 57, no. 15, 2020, Art. no. 151203, doi: 10.3788/lop57.151203.

[32] Y. Hu, Z. Liu, D. Yang, and C. Quan, "Online fringe pitch selection for defocusing a binary square pattern projection phase-shifting method," *Opt. Exp.*, vol. 28, no. 21, pp. 30710–30725, Oct. 2020, doi: 10.1364/oe.409046.

Jiangping Zhu received the Ph.D. degree in optical engineering from the Institute of Optics and Electronics, Chinese Academy of Sciences, Chengdu, China, in 2014.

In 2018, he was a Visiting Scholar with Harvard University, Cambridge, MA, USA. He is currently an Associate Professor with the College of Computer Science, Sichuan University, Chengdu. He is the author of more than 50 journal articles and has written eight patents. His research interests include computer vision, microscopy shape detection, and 3-D imaging.

Changhui Zhu received the B.S. degree in engineering management from Sichuan University, Chengdu, China, in 2018, where she is currently pursuing the M.S. degree in software engineering.

Her research interests include computer vision and 3-D structured light measurement and pattern binary encoding.

Pei Zhou received the B.E. degree from Wuhan University, Wuhan, China, in 2011, the M.E. degree from the Chinese Academy of Science, Chengdu, China, in 2014, and the Ph.D. degree from Sichuan University, Chengdu, in 2020.

From 2014 to 2016, she was a Software Research Engineer at Huawei, Chengdu. She is currently a Post-Doctoral Researcher with the College of Computer Science, Sichuan University. Her research interests include machine vision and optical 3-D measurement and its application.

Zhoumiao He is currently pursuing the Ph.D. degree in software engineering with the School of Computer Science, Sichuan University, Chengdu, China.

Her research interests involve 3-D shape measurement and structured light measurement.

Di You is currently pursuing the Ph.D. degree with National Key Laboratory of Fundamental Science on Synthetic Vision, Sichuan University, Chengdu, China.

His current research interests include computer vision and machine learning.